Brownian dynamics simulation of gelation and aging in interacting colloidal systems

Martin T. A. Bos

Department of Physical and Colloid Chemistry, Wageningen Agriculutural University,
Dreijenplein 6, 6703 HB Wageningen, The Netherlands

Joost H. J. van Opheusden

Department of Agricultural Engineering and Physics, Wageningen Agricultural University,
Bomenweg 4, 6703 HD Wageningen, The Netherlands

(Received 30 May 1995)

In this paper we simulate the aggregation of interacting particles using Brownian dynamics. The parameters varied are volume fraction and interaction potential well depth. At volume fractions above 0.07 percolated structures are observed; these are formed differently from cluster-cluster aggregation. Fractal analysis of the structures shows nonuniversal fractal scaling for all systems, with lower bound r_0 and fractal dimensionality d_f. Both of these properties depend on the simulation parameters and on time. Compactification in time leads to an increasing r_0 and a decreasing d_f, that is, structures with thick strands. This effect is most pronounced at large well depths. Due to compactification in time, percolated states can be transient.

PACS number(s): 62.43.Hv, 61.20.Ja, 82.70.Gg, 61.20.Lc

I. INTRODUCTION

Lyophobic colloids can be stabilized by charging the surface of the dispersed particles. Alternatively, a layer of polymer with high affinity for the solvent can be applied to the particle surface, resulting in steric stabilization. If the stabilization is taken away, the colloidal particles will aggregate: particles that collide through Brownian motion will form a cluster. At first, clusters are held together by relatively weak attractive forces (e.g., Van der Waals forces) between the particle surfaces. On a larger time scale, aging and inserting lead to more rigid clusters.

A laboratory example of aggregation is the destablization of carboxyl-stabilized latex particles dispersed in water. Under alkaline conditions, the particles in this system carry charged groups. Addition of the acid glucono-δ-lactone removes the charges, resulting in aggregation. Steric destabilization can be found in cheese making, where rennet is added to a dispersion of casein micelles in an aqueous medium ("skim milk"). Here the enzyme removes the stabilizing layer of κ casein.

For a lyophobic colloid consisting of homodisperse solid spherical particles, the structure that minimizes the free energy is a close-packed cluster. On the other hand, in most systems particles are actually brought together by Brownian diffusion, resulting in ramified clusters. Therefore, the development of the structure in time is determined by a competition between Brownian diffusion and reorganization of clusters to a more close-packed structure. Both processes can have different time scales depending on the system used.

In the aggregating systems mentioned above, the resulting structures are often far from close packed. Figure 1 gives a micrograph of an aggregated system of Teflon latex particles, showing a cloudy network of cross-linked ramified clusters. Here, at a relatively low volume fraction ($\varphi = 0.025$), a percolated structure is formed that cannot reorganize easily to a close-packed aggregate. If bonds between particles become rigid due to aging and sintering, reorganization becomes im-

possible, and no close-packed clusters will be formed.

An important question for many colloidal systems is which structures will be formed upon destabilization, and what dynamics lead to them. Destabilization of colloids has been modeled as phase separation [1–3]. Using density-functional theory, the development in time of an initially uniform density pattern can be written in the form of a diffusion equation. This diffusion equation is of no use when inhomogeneities on many length scales are to be modeled over longer time scales; a mean-field theory is inadequate for describing structures such as those in Fig. 1.

Aggregation of hard-core particles to irregular structures has been studied extensively in computer simulations [4,5] (more recently [5,7]) and experiments [8–13] using fractal models to describe aggregated structures. In many simulations, clusters are regarded as rigid entities, which are treated as particles with scaled diffusion and interaction behavior. Following this scheme, aggregation by diffusion has been studied, although cluster reorganization has been taken into account by allowing reversible aggregation [14], desorption of particles form clusters [15], or by deformations of aggre-
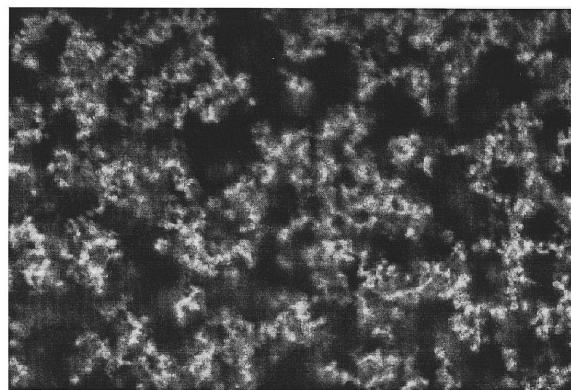

FIG. 1. Aggregated 100-nm Teflon latex particles (white). The micrograph represents 132×89 μm.

53   5044

gates [7]. The behavior of these systems under shear has received much attention in theory [16], simulation [17], and experiment [18].

In this article we present the results of a Brownian-dynamics simulation of aggregating Lennard-Jones particles, in which both cluster growth and cluster reorganization occur simultaneously, and all particles are considered explicitly. The resulting structures will be interpreted using fractal models.

II. BROWNIAN DYNAMICS

A. The model

In the simulation, we keep track of the coordinates of N particles in three dimensions. The Brownian-dynamics method [19,20] is based on the Langevin equation:

$$\mathbf{F}_{\text{res}} = m\frac{d^2}{dt^2}\mathbf{r}_i = \sum_j \mathbf{I}_{ij}(r_{ij}) + \mathbf{R}_i + \mathbf{H}_i. \tag{1}$$

Equation (1) gives the resulting force on particle i with mass m, where $\mathbf{I}$ is the force modeling interaction between particles, $\mathbf{R}$ the force modeling diffusion, and $\mathbf{H}$ the force modeling hydrodynamic interactions. Equation (1) is a coupled system of differential equations that can only be solved numerically. The solution gives the particle trajectories.

We approximate hydrodynamic interactions by simple Stokesian friction (i.e., hydrodynamic interactions between particles are neglected),

$$\mathbf{H}_i = 3\pi\eta\sigma\frac{d\mathbf{r}_i}{dt}, \tag{2}$$

with η the viscosity of the continuous phase and σ the diameter of the particles. Diffusion is modeled by a stochastic force that mimics collisions between particles and solvent molecules.

Equation (1) is solved numerically using a constant time step Δt. We choose this time step to be much larger than the relaxation time for one stochastic pulse, and neglect the inertia term, the second-order term in (1). This reduces (1) to a first-order differential equation:

$$\frac{d}{dt}\mathbf{r}_i = \frac{1}{3\pi\eta\sigma}\left[\sum_j \mathbf{I}_{ij} + \mathbf{R}_i\right]. \tag{3}$$

We solve (3) using the Euler forward method [21]:

$$\Delta\mathbf{r}_i(t+\Delta t) = \frac{\Delta t}{6\pi\eta a}\left[\sum_j \mathbf{I}_{ij}(t) + \mathbf{R}_i(t)\right]. \tag{4}$$

To avoid inaccuracy, Δt must be chosen small enough to ensure that the interaction forces do not change significantly during one integration step. Values for Δt will be given in the next section.

The stochastic displacement, which is the effect of $\mathbf{R}$, is tuned to obey Einstein's law for an isolated particle:

$$\Delta x_i^R(t+\Delta t) = G_q\sqrt{2kT\Delta t/3\pi\eta\sigma}. \tag{5}$$

G_q is a Gaussian distributed random number with unity variance. The index q indicates that different random numbers

are drawn: three random numbers to calculate the stochastic displacement vector for one particle; $3N$ random numbers for the whole system in one time step. This ensures that in the absence of interactions, the displacement vectors over different particles and times are uncorrelated. In the absence of interactions, the system will asymptotically obey Einstein's law.

As the average resultant force on a particle is always zero (neglect or inertia), the energy of the particles must remain constant. This means that the energy required for the stochastic displacements is completely dissipated by friction. As both the stochastic term and the friction term in the Langevin equation describe interactions with solvent molecules, we can conclude that in the absence of interactions, the solvent temperature T also remains constant.

In the presence of interactions, the system has not only thermal but also potential energy, with total amount V_{sys}:

$$V_{\text{sys}} = \sum_{i\neq j} U_{ij}(r_{ij}), \tag{6}$$

where U_{ij} is the potential energy for a particle pair as a function of their separation r_{ij}. In one interval Δt, the system will decrease V_{sys} when possible by particle displacement. Again, the decrease in V_{sys} is converted solely to friction energy, which would normally result in a rise in solvent temperature. In this simulation, however, we keep T constant, which amounts to thermostatting the sample. This is very well imaginable, as the decrease in V_{sys} is typically a slow process.

In this model interactions are described using the Lennard-Jones potential,

$$U_{ij}(r_{ij}) = 4\varepsilon\left[\left(\frac{\sigma}{r_{ij}}\right)^{12} - \left(\frac{\sigma}{r_{ij}}\right)^6\right], \tag{7}$$

in which ε is the attraction energy at the minimum of U_{ij} and σ is the distance at which U_{ij} changes from attractive to repulsive. The minimum in U_{ij} lies at $r_{ij} = 2^{1/6}\sigma$. The interaction force follows from the gradient of the interaction potential. Lennard-Jones particles are "soft," i.e., it is possible to find a pair of particles at a separation smaller than σ. We use σ as the hydrodynamic diameter in the free-draining limit of (2). To increase computational speed, U_{ij} is taken to be zero at distances higher than 2.5σ.

In this work we investigate the effects of attractive interparticle interactions in the simplest form by using a potential with few parameters. The Lennard-Jones potential meets this criterion well, but is unrealistic in describing interactions between real colloidal particles. For the moment, however, we postpone a study using complicated but more realistic potentials, and restrict ourselves first to the effects of a simple potential. A great advantage of the Lennard-Jones potential is the fact that its equilibrium phase diagram is known. This means that although equilibrium may not be reached during the simulation, values for ε can be placed in a thermodynamical perspective.

TABLE I. Absolute time scales in the simulation.

σ (nm)	Δt (μsec)	$\Delta t/\tau_r$
10	0.003 44	618.79
10^2	3.44	6187.9
10^3	3440	61879

B. Parameters in Brownian dynamics

In the simulation, all distances are normalized to σ and all energies to kT. Equation (5) can be written in dimensionless form,

$$\Delta \tilde{x}_i^R(t+\Delta t) = G_q\sqrt{\tilde{S}}, \tag{8}$$

where the tilde signifies a dimensionless quantity and $\tilde{S}$ is given by

$$\tilde{S} \equiv \frac{2kT\Delta t}{3\pi\eta\sigma^3}. \tag{9}$$

$[\tilde{S}]^{1/2}$ is the dimensionless rms particle displacement in the absence of interactions. The value of $[\tilde{S}]^{1/2}$ has been 0.003 in all simulation runs; this ensures that most displacements will be small relative to the particle size and that interactions forces will not change too much during one integration step.

The consequences of this choice for varying particle diameters are shown in Table I, for a system of polystyrene particles (density 1000 kg/m^3) dispersed in water (viscosity 10^{-3} Pas) at 298 K:

The third column contains the ratio of Δt and the relation time for one stochastic pulse:

$$\tau_r = \frac{m}{3\pi\eta\sigma}. \tag{10}$$

Table I shows that for these systems inertia effects can indeed be neglected.

The only parameters left for varying are N, the number of particles in the system, $\tilde{\varepsilon}$, the well depth in (7) normalized to kT, and the volume fraction φ. As we are interested in irreversible aggregation, we shall choose these parameters in the unstable region of the Lennard-Jones phase diagram.

A starting configuration of a given volume fraction is generated by placing N particles at random in the simulation box at very low volume fraction (φ of order 10^{-5}), and then performing a simulation where the particle positions are rescaled by a factor $[\tilde{S}]^{1/2}$ after every ten random displace-

ments. This is continued until the desired volume fraction is reached. The resulting configuration is equilibrated under repulsive Lennard-Jones interactions, i.e., U_{ij} is set to 0 for $r_{ij} \geq 2^{1/6}\sigma$ to remove any ordering induced by the "growing" particles.

III. FRACTAL PROPERTIES

Fractal structures in colloids can arise by cluster-cluster aggregation (CCA), where particles aggregate to clusters, which then aggregate similarly on a larger length scale. A system undergoing CCA consists of clusters that are fractals, and can be characterized by a fractal dimensionality d_f and a proportionality constant $\tilde{n}$:

$$n(r) = \tilde{n}\left(\frac{r}{\sigma}\right)^{d_f}, \tag{11}$$

where $n(r)$ is the number of particles in one cluster of radius r. The fractal dimensionality characterizes the factor by which $n(r)$ increases upon an increase in cluster size. The smaller d_f is, the more ramified clusters become as they grow. For a system of fractal aggregates, $n(r)$ can also be interpreted as the average number of particles within a test sphere of radius r. When r is in the fractal scaling region, Eq. (11) holds. CCA has been studied extensively by computer simulation [4,5]; the resulting clusters show universal fractal behavior with a d_f of 1.75 at large aggregation probability (diffusion-limited aggregation) or 2.0 at small aggregation probability (reaction-limited aggregation).

To measure the fractal properties of our results, we study the integrated pair correlation function:

$$n_c(r) = 4\pi\rho_0 \int_0^r l^2 g(l)dl. \tag{12}$$

$n_c(r)$ is the average number of particles within range r of another particle. We measure d_f by identifying a linear region in a double logarithmic plot of $n_c(r)$, and applying a least-squares fit to this region. This is equivalent to studying the scaling of the pair correlation function [4], but tends to smooth out oscillations in $g(r)$. At large length scales $n_c(r)$ is only determined by the overall volume fraction: $g(r)$ then equals 1 and d_f becomes 3. We will call this the homogeneous scaling region.

For colloidal aggregates, the fractal scaling region will also have a lower bound r_0, typically of the order of the particle size. We can include this lower bound in the descrip-
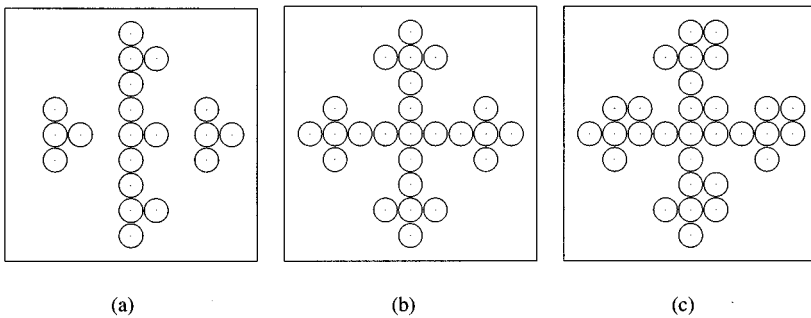

FIG. 2. Deterministic fractals.

TABLE II. Backbone parameters for fractals of Fig. 2.

Figure	$\widetilde{n}$	r_0/σ
2(a)	2.208	0.329
2(b)	$2.761 = 2^{d_t}$	0.500
2(c)	3.313	0.703

tion of $n(r)$ by assuming that on length scales equal to and larger than r_0, the aggregate structure is fractal, while below r_0 the aggregate structure is closely packed. This simplification will serve as a first approximation in determining values for r_0. The first assumption can be written as

$$\frac{n(r)}{n_0} = \left(\frac{r}{r_0}\right)^{d_f}, \tag{13}$$

where a cluster of radius r_0 contains n_0 particles. The second assumption can be written as

$$n_0 = 8\varphi_{\rm cp}\left(\frac{r_0}{\sigma}\right)^3 \tag{14}$$

in which $\varphi_{\rm cp}$ is the volume fraction of close packing. Substitution of (11) and (14) in (13) gives an expression for $\widetilde{n}$,

$$\widetilde{n} = 8\varphi_{\rm cp}\left(\frac{r_0}{\sigma}\right)^{3-d_t}, \tag{15}$$

from which we see that $\widetilde{n}$ is determined by both r_0 and d_f. To clarify this, we give an example of values for $\widetilde{n}$ and r_0 for three deterministic fractals in two dimensions. All fractals have d_f, ln5/ln3; only the backbone is different:

In Fig. 2 only a small part of the fractals is shown; the rest of the fractal repeats this part self-similarly. Note that Fig. 2(a) constitutes a fractal object, even if it does not form a connected cluster. By writing $n(r)$ as a series, $\widetilde{n}$ can be easily obtained numerically. r_0 is calculated from $\widetilde{n}$ using (15), assuming $\varphi_{\rm cp}$ to be 1. The results are given in Table II.

Here we see that our choice for $\varphi_{\rm cp}$ gives for case (b) the value for r_0 that we would expect intuitively: the particle radius. Both $\widetilde{n}$ and r_0 quantitatively reflect the differences in backbone, regardless of the size of the fractal.

As far as the authors know, the notion of the backbone parameters $\widetilde{n}$ and r_0 is a new concept in experimental and simulational studies concerning the fractal structure of aggre-
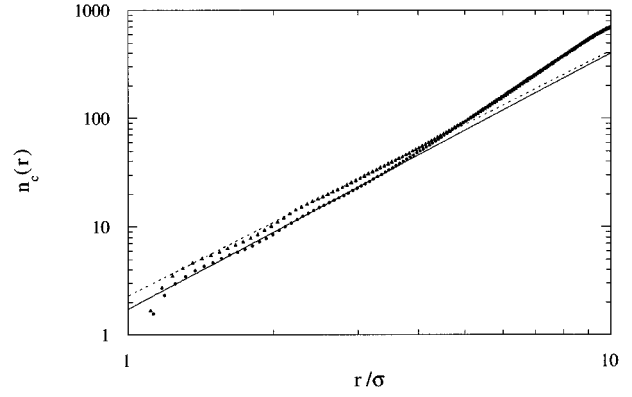

FIG. 3. $n_c(r)$ plot of an aggregating system. Dots, after 100 000 iterations; triangles, after 350 000 iterations.

gating systems. Until now, all attention has been focused on measuring and interpreting the fractal dimensionality.

IV. RESULTS AND DISCUSSION

A. Fractal results

An example of an $n_c(r)$ plot for $\varphi = 0.13$ and $\varepsilon = 2$ is given in Fig. 3. The particle volume fraction φ is calculated using $2^{1/6}\sigma$ as the hard sphere diameter.

In Fig. 3 we see that the fractal scaling region is very small. For this system the homogeneous scaling region already sets in at four to five particle diameters, which makes a least-squares fit to some extent arbitrary and the scaling results no more than semiquantitative. The oscillations in $n_c(r)$ at small r are caused by excluded volume effects. The fractal scaling region grows in time.

From Fig. 3 it follows that the proportionality constant $\widetilde{n}$ increases with time. Equation (15) shows that we can interpret an increasing $\widetilde{n}$ as an increase in size of the close-packed building blocks of fractal clusters, i.e., compactification.

In evaluating $\widetilde{n}$ for our simulation, we have to correct for using the Lennard-Jones diameter σ instead of the distance of lowest U_{ij}, $2^{1/6}\sigma$. Hence we use for φ_0 in (15) the volume fraction of fcc close-packed particles, 0.76, divided by $\sqrt{2}$.

In Figs. 4 and 5 we show the results for d_f and r_0 for three volume fractions. From Figs. 4 and 5 it is clear that there is no universal fractal behavior in the aggregated sys-
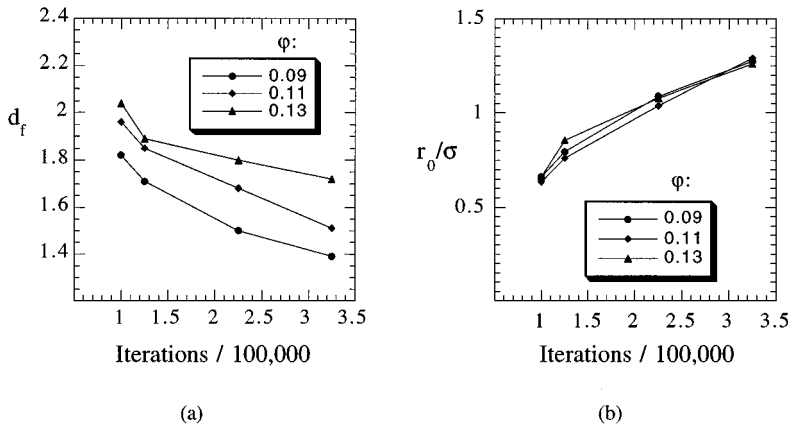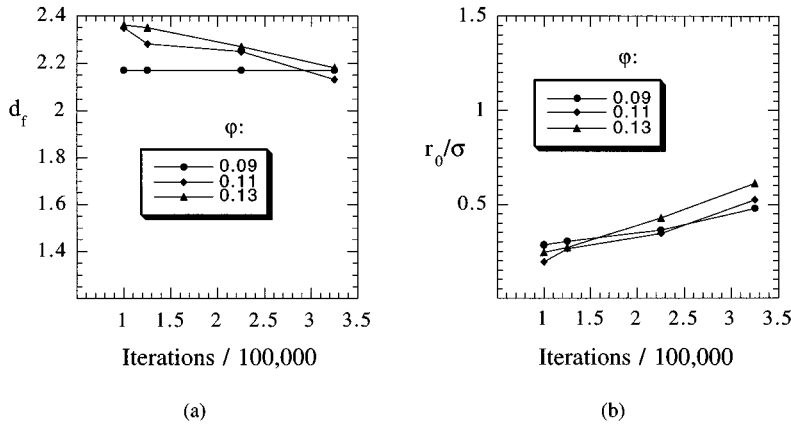

(a)

(b)

FIG. 4. Fractal parameters for $\varepsilon = 4$.

FIG. 5. Fractal parameters for $\varepsilon = 2$.

(a)

(b)

tems studied here. Generally, d_f decreases with time, indicating more stringlike clusters. Also, r_0 increases with time, indicating compactification.

In many studies, compactification is automatically associated with an increasing d_f. These data, however, show that the measured dimensionality need not be relevant to the length scales on which compactification occurs. In this article, d_f always describes length scales larger than r_0. A compactification on short length scales in a connected network must result in a more open structure on intermediate length scales, hence the decreasing d_f.

The values of d_f and r_0 depend on both volume fraction and well depth. Compared to Fig. 4, d_f in Fig. 5 starts at a higher value and decreases more slowly; r_0 in Fig. 4 starts at a higher value than in Fig. 5 and increases faster.

B. Discussion: Higher volume fractions

We have studied cluster statistics of the system with $U_{ij} < -kT$ as a connectivity criterion. The simulated systems with φ higher than 0.09 form percolated clusters. An example of such a cluster is given in Fig. 6(a), where only the particles belonging to the cluster are shown. Compactification in time causes percolating clusters to be transient. This is illustrated in Fig. 6(b), where compactification has caused a branch in the largest cluster to break. The largest cluster still percolates; after more iterations we find that percolating

clusters break up into loose clusters. The reorganization we see in Fig. 6 is in accordance with a decreasing d_f and an increasing r_0.

To understand the mechanism by which percolation occurs, we studied a larger system ($N = 10\,000$) using the same parameters. After 25 000 iterations, 80% of all the particles were already in one cluster. This cluster is drawn in Fig. 7(a). It appears that the system is separated into connected regions with high particle concentration (the cluster) and low particle concentration (voids). Figure 7(a) somewhat resembles that initial structure of phase-separating liquids [1], in which both phases form percolated networks.

In the simulation, the number of particles contained in this cluster decreases with time. After 200 000 iterations, the largest cluster contains only 10% of all the particles. The resulting cluster, drawn in Fig. 7(b), has become more compact at small length scale, but has retained its percolative properties. From Fig. 7(a) to Fig. 7(b) the cluster has compactified significantly, leaving thin branched strands between larger voids.

We find that a greater well depth merely seems to speed up the processes described above. At high, ε a percolated cluster is formed faster, but reorganization is also faster (though not necessarily in the same proportion). At lower ε, the clusters look less closely packed. At ε of order kT, we observed no percolation in these systems.

For the percolated systems we have calculated the pressure in the system [21]. We found $(PV/NkT) - 1$ typically to
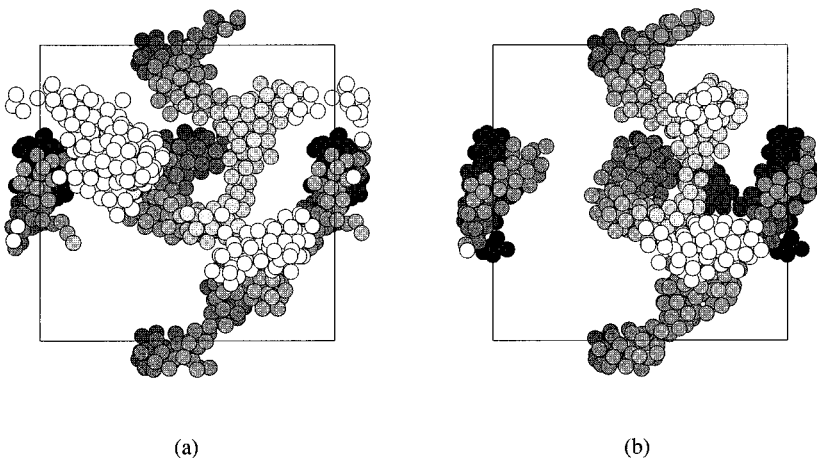
FIG. 6. Largest cluster for $N = 1000$; $\varphi = 0.093$; $\varepsilon = 4$. In these three-dimensional configuration snapshots shading is used as depth cuing.
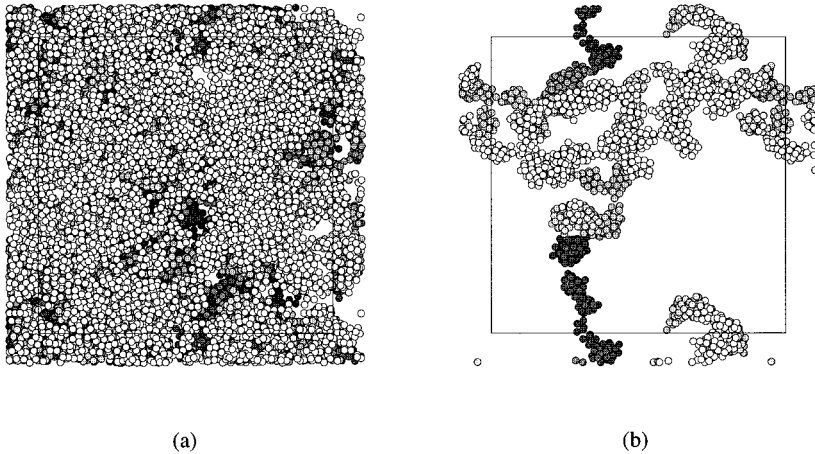
(a)

(b)

FIG. 7. Largest cluster for $N = 10\,000$; $\varphi = 0.093$; $\varepsilon = 4$.

(a)   (b)

be of order -10^{-7}, implying a very small underpressure caused by the network pulling on itself. To investigate directional effects, we calculated the stress tensor: the stress contribution of the nondiagonal terms was about 2% of the contribution of the diagonal terms, and positive. None of these results indicate that percolation is an artifact of the simulation.

C. Lower volume fractions

For volume fraction 0.074 we both started and ended up with loose, nonpercolating clusters. At well depth $\varepsilon = 2$ one cluster was found with a linear shape, as given in Fig. 8. Closer inspection of the simulation data showed that this cluster was formed by aggregation of several smaller clusters. The formation of this strandlike cluster differs from that described in the preceding section. Here the number of particles contained in the largest cluster increases with time. As in the preceding section, a larger ε leads to more closely packed clusters. At $\varepsilon = 4$, we only find small compact clusters with a variety of elongated shapes, which are probably the effect of rotational diffusion. When a dimer rotates, the connection probability for a third approaching particle is larger at the two ''tips'' of the dimer than near the center of gravity. This simulation includes rotational diffusion for
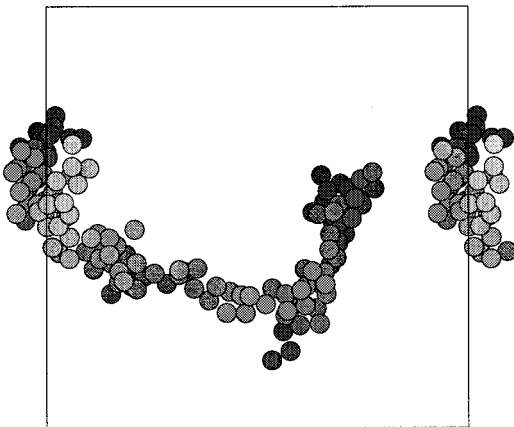
clusters, as the sum of all the particle displacements in a cluster causes both translation and rotation of the cluster as a whole.

V. CONCLUSIONS

For aggregating Lennard-Jones systems we find percolating networks at volume fractions above $\varphi = 0.07$. These networks appear to be formed by reorganization of large aggregates, during which branched strands are formed with voids in between. During this reorganization, the number of particles in the largest cluster decreases. Fractal analysis gives nonuniversal results, which is not surprising, since the mechanism of aggregation differs from CCA: both diffusion and reorganization determine the aggregated structure. Still, significant scaling regions are found. The effect of reorganization on the fractal parameters is a decreasing d_f and an increasing r_0.

At lower volume fractions, aggregation of clusters has been observed, but no percolating networks have been found. Apparently, the region in which percolating structures are formed as described in bounded by a lower volume fraction; below this bound there is competition between cluster growth and cluster reorganization, which the latter wins in most of the simulations. However, it is very likely that there is a region in which cluster growth prevails. If we denote such a region by CCA, the region of loose clusters by L, and the percolated region by P, we can sketch a diagram in parameter space, which is done in Fig. 9. This diagram is

FIG. 8. Largest cluster for $N = 1000$; $\varepsilon = 0.074$; $\varepsilon = 2$.
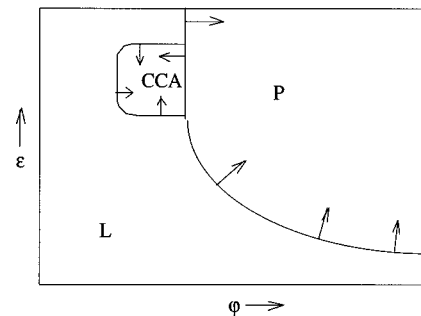

FIG. 9. Regions in parameter space, all units arbitrary.

higher speculative, but rather generally based on the mechanisms found in this paper.

The diagram drawn is not a phase diagram, as all structures are transient due to reorganization. This is indicated by arrows showing how the ''coexistence lines'' will advance in time. In the P region, the attractive interaction forces cause in time both formation and fracture of percolating clusters.

The Lennard-Jones potential strongly favors reorganization, as it has a very broad interaction range. More realistic (i.e., short-range) interaction potentials will drastically alter the diagram. Also, in real systems, roughness of particle and sintering can freeze in structures. However, the notion of different mechanisms to obtain percolated structures (CCA and P) helps one to understand the structures that can be expected at different volume fractions and interaction potentials. A computer simulation where particles are considered explicitly is necessary to sample other regions in the ''phase diagram'' than the CCA region. Our next aim is to use Brownian dynamics to simulate systems with short-range potentials and to include effects of sintering.

ACKNOWLEDGMENTS

[1] J. W. Cahn, J. Chem. Phys. **42**, 93 (1965).

[2] H. Löwen, Phys. Rep. **337**, 249 (1993).

[3] W. Li and J. C. Lee, Physica A **202**, 165 (1993).

[4] T. Vicsek, *Fractal Growth Phenomena* (World Scientific, Singapore, 1992).

[5] P. Meakin, in *Phase Transitions and Critical Phenomena*, edited by C. Domb and J. L. Lebowitz (Academic, New York, 1987), Vol. 12.

[6] P. Meakin, J. Colloid Interface Sci. **134**, 235 (1990).

[7] H. F. van Garderen *et al.*, J. Chem. Phys. **102**, 480 (1995).

[8] D. A. Weitz and M. Oliveira, Phys. Rev. Lett. **52**, 1433 (1984).

[9] G. Dietler, C. Aubert, and D. S. Cannell, Phys. Rev. Lett. **57**, 3117 (1986).

[10] P. W. Rouw and C. G. de Kruif, Phys. Rev. A **39**, 5399 (1989).

[11] L. G. B. Bremer *et al.*, Adv. Colloid. Interface Sci. **46**, 117 (1993).

[12] M. Carpinetti and M. Giglio, Adv. Colloid. Interface Sci. **46**, 73 (1993).

[13] P. W. Zhu and D. H. Napper, Phys. Rev. E **50**, 1360 (1994).

[14] M. Kolb, J. Phys. A **19**, L263 (1986).

[15] W. Y. Shih, I. A. Aksay, and R. Kikuchi, Phys. Rev. A **36**, 5015 (1987).

[16] A. A. Potanin, J. Chem. Phys. **96**, 9191 (1992).

[17] A. H. L. West, J. R. Melrose, and R. C. Ball, Phys. Rev. E **49**, 4237 (1994).

[18] R. de Rooij *et al.*, Phys. Rev. E **49**, 3039 (1994).

[19] D. M. Heyes, J. Non-Newt. Fluid Mech. **27**, 47 (1988).

[20] J. M. van der Veer, Ph.D. thesis, University of Twente, The Netherlands, 1992.

[21] M. P. Allen and D. J. Tildesley, *Computer Simulation of Liquids* (Oxford University Press, Oxford, 1993).